

Signatures of the orbital angular momentum of an infrared light beam in the two-photon transition matrix element: A step toward attosecond chronoscopy of photoionization

Sucharita Giri,¹ Misha Ivanov,^{2,3,4} and Gopal Dixit^{1,*}

¹*Department of Physics, Indian Institute of Technology Bombay, Powai, Mumbai 400076 India*

²*Max-Born-Institut, Max Born Strasse 2A, 12489 Berlin, Germany*

³*Blackett Laboratory, Imperial College London, South Kensington Campus, SW7 2AZ London, United Kingdom*

⁴*Department of Physics, Humboldt University, Newtonstrasse 15, 12489 Berlin, Germany*

Abstract

We present a theory of time-resolved photoionisation in the presence of a vortex beam. In a pump-probe setup, an extreme ultraviolet or an x-ray pump pulse triggers ionization, which is probed by a synchronized infrared pulse with non-zero orbital angular momentum. We show, how this property of the probe pulse affects the electron dynamics upon ionization, in a way that is independent of the initial and final angular momentum states of the ionizing system.

PACS numbers:

INTRODUCTION

In their pioneering work, Allen and co-workers have shown the existence of the orbital angular momentum (OAM) of a light beam, along with its spin angular momentum [1]. The OAM of light is related to the spatial profile of the light beam and is characterized by the topological charge l , which can have only integer values from 0 to $\pm\infty$, whereas the spin angular momentum is related to the polarization properties of light. Since its first demonstration, the OAM of light has found numerous macroscopic applications in different fields [2–4] including quantum information processing [5], optical interferometry [6], chiral recognition in molecules [7–9], manipulation of nanoparticles [10] and in quantum gases [11, 12]. While it is relatively straightforward to generate beams with non-zero orbital angular momentum in the infrared (IR) and visible range, similar technology is much more difficult in the extreme ultraviolet (XUV) and x-ray range. This has stimulated recent works on using high-harmonic generation to up-convert OAM beams from the IR to the XUV and soft x-ray energy range [13–21]. An elegant non-collinear scheme has been employed to generate linearly polarized twisted light beams with relatively low OAM [22–24] via high-harmonic generation. These breakthroughs have opened a door to synthesize coherent attosecond XUV and x-ray pulses with desirable OAM properties, adding an additional knob to the attosecond light generation toolbox.

It may appear that, apart from the space-dependent amplitude and phase modulation, the macroscopic OAM properties of an IR or visible light beam will hardly manifest at the single-atom, microscopic level due to the difference in the spatial scales. As long as the dipole approximation dominates the atomic response, each atom sees a local field at a given spatial position inside the OAM beam. However, this general impression is not always accurate, as shown in particular in [25], using a Bose-Einstein condensate with naturally delocalized centre-of-mass atomic wavefunction. Here we analyse an alternative possibility and show how the topological charge of an incident OAM IR beam can be encoded via attosecond chronoscopy of photoionisation [26] by a pair of time-synchronized x-ray pump and IR probe pulses. Attosecond streaking and RABBITT (reconstruction of attosecond beating by interference of two-photon transitions) are the most common experimental methods to perform attosecond chronoscopy of photoionization [26].

In our proposed scheme, an attosecond x-ray pump pulse ionises atoms (shown in blue

colour in Fig. 1). The liberated photoelectrons are probed by a twisted IR probe pulse (shown in pink). The short wavelength of the pump pulse allows one to focus it tightly into the centre of the OAM doughnut, where the amplitude and the phase structure of the twisted IR probe can be experienced by the photoelectrons. In the generalised theory of time-resolved photoionisation, both the pump and probe pulses can carry OAM. However, for our purpose, we limit the analysis to the case when the X-ray pump pulse has no OAM but the IR probe can carry OAM. The fact that the X-ray pump pulse does not have to carry OAM, simplifies practical realisation of the proposed setup using currently developing X-ray sources.

As shown by Picon and co-workers [27, 28], when the phase and amplitude inhomogeneity of a twisted beam becomes important, the standard dipolar selection rules are no longer adequate [29]. Exchange of angular momentum larger than one unit has been found during photoionisation [27, 28] and photoexcitation of valence electrons with twisted beams [4, 25, 30, 31]. Attosecond time-delay in photoionisation has been predicted to be sensitive to the magnetic sublevels of a spherically symmetric atom ionised by a twisted XUV beam [32].

There is an important difference between all-optical setups, which detect light generated by matter interacting with OAM beams, and setups detecting photoelectrons. In the former case, the OAM properties of the incident light are recorded across a macroscopic sample and affect the measurement via coherent addition of the optical response from different parts of the interaction region. While measuring photoelectrons, OAM-sensitive signal arises when an atom is placed near the centre of the twisted beam, where amplitude and phase modulation is maximised (at the expense of low incident field intensity).

THEORY

In the time-resolved photoionization, within the pump-probe scenario, the pump pulse liberates an electron from the ground state $|i\rangle$ with negative energy ϵ_i . The electron is promoted to a continuum state $|k'\rangle$ with energy $\epsilon_{k'}$. The photoelectron is probed by the twisted IR pulse, which induces a transition from a continuum state $|k'\rangle$ to another continuum state $|k\rangle$ with energy ϵ_k . In the following, we present the theory of time-resolved photoionization.

First, we write the two-photon transition amplitude corresponding to the absorption of

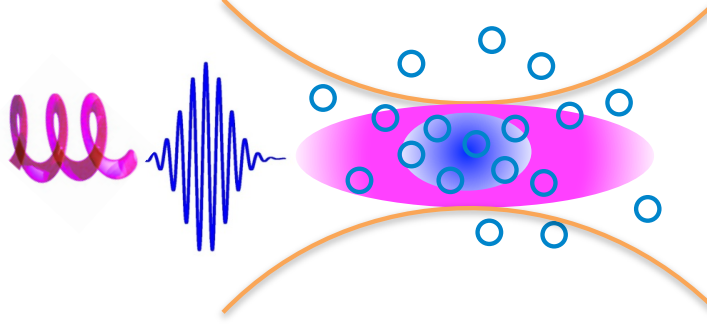


FIG. 1: Schematic of time-resolved photoionization by a pair of regular x-ray pump pulse with zero orbital angular momentum (shown in blue) and a twisted infrared probe pulse (shown in pink). The focal volumes of both pulses are shown by their respective colours, atoms are depicted with blue open circles. The x-ray pump pulse ionizes the electrons from the atoms and the liberated photoelectrons, within the focal volume, are probed by the twisted infrared pulse.

both one pump and one probe photons,

$$M_{\epsilon_k, \epsilon_i}^{(2)} = i \lim_{\delta \rightarrow 0} \int_0^\infty d\epsilon_{k'} \frac{\langle k | \mathcal{H}_{\text{int}} | k' \rangle \langle k' | \mathcal{H}_{\text{int}} | i \rangle}{(\epsilon_{k'} - \epsilon_i - \Omega - i\delta)}. \quad (1)$$

Here, the energy of the final continuum state is $\epsilon_k = \epsilon_i + \Omega + \omega$, where Ω and ω are the photon energies of the pump and IR probe pulses, respectively. The pump photon energy is larger than the ionization potential of the atomic system.

The interaction Hamiltonian is $\mathcal{H}_{\text{int}} = -\hat{\mathbf{A}}(\mathbf{r}, t) \cdot \hat{\mathbf{p}}$ where $\hat{\mathbf{A}}(\mathbf{r}, t)$ is the vector potential of the pump and IR probe pulses. The vector potential corresponding to the probe vortex pulse, which induces a transition from $|k'\rangle$ to $|k\rangle$, has the following form [28]

$$\mathbf{A}(\mathbf{r}, t) = \mathbf{A}_0 w_0 g(t) [e^{i(\mathbf{k} \cdot \mathbf{r} - \omega t)} \text{LG}_{l,p}(\rho, \phi, z; \mathbf{k}) + \text{c.c.}]. \quad (2)$$

Here, \mathbf{A}_0 is the amplitude (including polarization state), w_0 is the beam waist of the pulse, $g(t)$ is the envelope of the pulse, \mathbf{k} is a carrier wave vector, ω is carrier frequency and $\text{LG}_{l,p}$ is the Laguerre-Gaussian modes of the pulse, which contains the transverse spatial structure of the vortex pulse with l and p corresponding to the topological charge and the radial node of the LG mode, respectively. In the present work, we have used the expression of $\text{LG}_{l,p}(\rho, \phi, z; \mathbf{k})$ as given in Eq. (2) of Ref. [28].

The ground state wavefunction is written as a product of the radial and angular parts, $\varphi_i(\mathbf{r}) = \langle \mathbf{r} | i \rangle = R_{n_i, l_i}(r) Y_{l_i, m_i}(\hat{r})$. The final continuum state wavefunction is expressed in

terms of the partial wave expansion as $\varphi_k(\mathbf{r}) = (8\pi)^{\frac{3}{2}} \sum_{l,m} i^l e^{-im} R_{k,l}(r) Y_{l,m}(\hat{r}) Y_{l,m}^*(\hat{k})$. The phase η_l is the scattering phase, i.e., the difference between the phase of the photoelectron ejected from the atom and that of a free-electron.

We substitute these expressions in the total two-photon amplitude Eq. (1), which reduces to the product of radial and angular parts

$$M_{\epsilon_k, \epsilon_i}^{(2)} \propto i(8\pi)^{\frac{3}{2}} A_\omega A_\Omega \sum_{l,m} \sum_{l',m'} (-i)^l e^{im} Y_{l,m}(\hat{k}) T_{l,l',l_i} \times \text{Angular part}, \quad (3)$$

where A_Ω and A_ω are, respectively, the amplitudes of the vector potentials of the pump and probe pulses and T_{l,l',l_i} is the radial part of the two-photon amplitude. The quantum numbers l_i , l' and l are the angular momenta of the initial ground, intermediate continuum and final continuum states. The range of accessible angular momenta for intermediate and final continuum states is decided by the selection rules. For vortex pulses, the selection rules are significantly different compared to the standard dipole selection rules [4, 27–29]. Here we assume that both pulses are linearly polarised along the quantization axis z .

The radial part of the two-photon transition amplitude $M_{\epsilon_k, \epsilon_i}^{(2)}$ is

$$T_{l,l',l_i} = \lim_{\delta \rightarrow 0} \int_0^\infty d\epsilon_{k'} \frac{\langle R_{k,l} | \mathcal{H}_{\text{int}}(r) | R_{k',l'} \rangle \langle R_{k',l'} | \mathcal{H}_{\text{int}}(r) | R_{n_i,l_i} \rangle}{(\epsilon_i + \Omega - \epsilon_{k'} + i\delta)}, \quad (4)$$

where $\mathcal{H}_{\text{int}}(r)$ is the radial part of the interaction Hamiltonian. We first compute the continuum-continuum (CC) transition amplitude, $\langle R_{k,l} | \mathcal{H}_{\text{int}}(r) | R_{k',l'} \rangle$, and then substitute the result for $\langle R_{k,l} | \mathcal{H}_{\text{int}}(r) | R_{k',l'} \rangle$ into the energy integral of Eq. (4), to obtain the compact form of T_{l,l',l_i} . We use the standard asymptotic form of the radial continuum wavefunction,

$$\lim_{r \rightarrow \infty} R_{k,l}(r) = \frac{1}{r} \sqrt{\frac{2}{\pi k}} \sin \left[kr - \frac{\pi l}{2} + \eta_l(k) + Z \frac{\ln(2kr)}{k} \right], \quad (5)$$

where $\eta_l(k)$ is the scattering phase-shift. It can be written as $\eta_l(k) = \sigma_l(k) + \delta_l(k)$ with $\sigma_l(k) = \arg[\Gamma(l+1 - iZ/k)]$, the Coulomb phase-shift and $\delta_l(k)$ originating from the short-range deviations of the ionic potential from a purely Coulombic form. In the asymptotic region, the phase of the continuum wavefunction also exhibits the standard logarithmic divergence characteristic for the Coulomb potential of the ionic core with charge Z . Note that the chosen form of the continuum wavefunction is not a good choice at low energy as shown in Ref. [33].

By using the expression of radial continuum wavefunction from Eq. (5), the CC radial

matrix element is

$$\begin{aligned} \langle R_{k,l} | \mathcal{H}_{\text{int}}(r) | R_{k',l'} \rangle &= \frac{2}{\pi \sqrt{k k'}} \left(\frac{\sqrt{2}}{w_0} \right)^{|l_2|} \int dr r^2 \frac{1}{r^2} \sin \left[kr - \frac{\pi l}{2} + \eta_l(\epsilon_k) + Z \frac{\ln(2kr)}{k} \right] \\ &\quad \times (r)^{1+|l_2|} \sin \left[k'r - \frac{\pi l'}{2} + \eta_{l'}(\epsilon_{k'}) + Z \frac{\ln(2k'r)}{k'} \right]. \end{aligned} \quad (6)$$

Here, $\mathcal{H}_{\text{int}}(r)$ is responsible for the CC transitions and depends on $|l_2|$, which is the topological charge of the vortex IR pulse. In the calculations, we have only retained the dominant term proportional to $\cos(k - k')$ and ignored the term proportional to $\cos(k + k')$. The simplified expression for the CC radial matrix element is

$$\begin{aligned} \langle R_{k,l} | \mathcal{H}_{\text{int}}(r) | R_{k',l'} \rangle &= \frac{1}{\pi \sqrt{k k'}} \left(\frac{\sqrt{2}}{w_0} \right)^{|l_2|} \lim_{\zeta \rightarrow 0} e^{i\Delta'} \frac{(2k')^{\frac{iZ}{k'}}}{(2k)^{\frac{iZ}{k}}} \left(\frac{i}{k' - k - i\zeta} \right)^{2+|l_2|+iZ\left(\frac{1}{k'} - \frac{1}{k}\right)} \\ &\quad \times \Gamma \left[2 + |l_2| + iZ \left(\frac{1}{k'} - \frac{1}{k} \right) \right] + \text{c. c.} \end{aligned} \quad (7)$$

Here, $\Delta = \eta_{l'}(k') - \eta_l(k)$ and $\Delta' = \Delta + \frac{\pi}{2}(l - l')$.

Substituting Eq. (7) in Eq. (4) and performing the complex energy integral near the pole corresponding to the energy $\epsilon_\kappa = \kappa^2/2 = \epsilon_i + \Omega$ yields the compact expression for T_{l,l',l_i}

$$\begin{aligned} T_{l,l',l_i} &= \frac{-i}{\sqrt{k\kappa}} \left(\frac{\sqrt{2}}{w_0} \right)^{|l_2|} \langle R_{\kappa,l'} | \mathcal{H}_{\text{int}}(r) | R_{n_i,l_i} \rangle \left(\frac{1}{|\kappa - k|} \right)^{2+|l_2|} \exp \left[-\frac{\pi Z}{2} \left(\frac{1}{\kappa} - \frac{1}{k} \right) \right] \\ &\quad \times (i)^{|l_2|} e^{i\Delta'} \frac{(2\kappa)^{\frac{iZ}{\kappa}}}{(2k)^{\frac{iZ}{k}}} \left(\frac{1}{\kappa - k} \right)^{iZ\left(\frac{1}{\kappa} - \frac{1}{k}\right)} \Gamma \left[2 + |l_2| + iZ \left(\frac{1}{\kappa} - \frac{1}{k} \right) \right]. \end{aligned} \quad (8)$$

In the above equation, the amplitude and phase terms are separated. The first line contains bound-continuum one-photon transition amplitude, whereas the second line **contains** the phase term of the CC transition amplitude whose strength is controlled by the exponential term.

After substituting the result of Eq. (8) in Eq. (3), the total two-photon transition amplitude reduces as

$$\begin{aligned} M_{\epsilon_k, \epsilon_i}^{(2)} &\propto -\frac{1}{\sqrt{k\kappa}} (8\pi)^{\frac{9}{2}} A_\omega A_\Omega \left(\frac{\sqrt{2}}{w_0} \right)^{|l_2|} \exp \left[-\frac{\pi Z}{2} \left(\frac{1}{\kappa} - \frac{1}{k} \right) \right] \\ &\quad \times \frac{1}{|k - \kappa|^{2+|l_2|}} \frac{(2\kappa)^{\frac{iZ}{\kappa}}}{(2k)^{\frac{iZ}{k}}} \left(\frac{1}{\kappa - k} \right)^{iZ\left(\frac{1}{\kappa} - \frac{1}{k}\right)} \Gamma \left[2 + |l_2| + iZ \left(\frac{1}{\kappa} - \frac{1}{k} \right) \right] \\ &\quad \times \sum_{l,m} \sum_{l',m'} (i)^{-l'+|l_2|} e^{i\eta_{l'}(\kappa)} Y_{l,m}(\hat{k}) \langle R_{\kappa,l'} | \mathcal{H}_{\text{int}}(r) | R_{n_i,l_i} \rangle. \end{aligned} \quad (9)$$

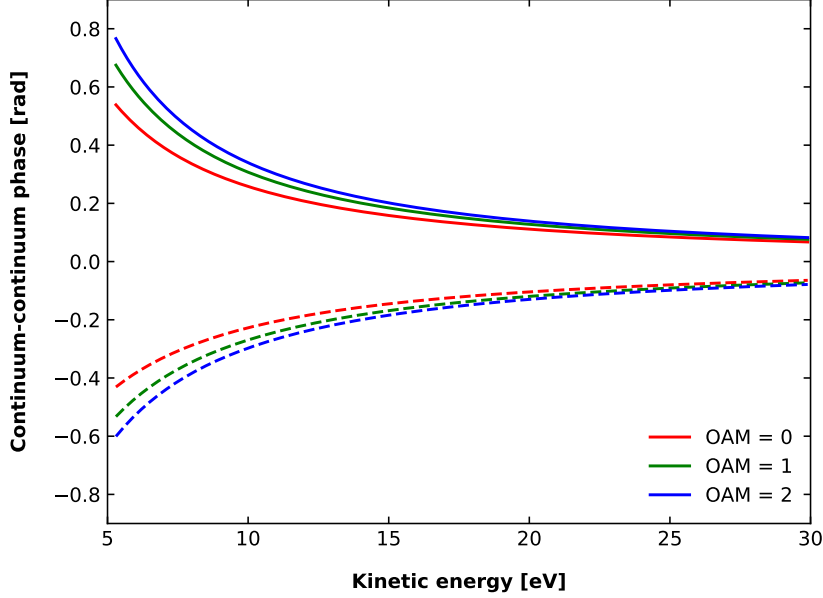


FIG. 2: The continuum-continuum quantum phases corresponding to absorption (solid lines) and emission (dotted lines) of the vortex IR pulse with different OAM values (topological charge $|l_2|$) for $\omega = 1.55$ eV and $Z = 1$. Here, OAM = 0 corresponds to regular IR pulse. The legend represents the solid curves from bottom to top and the dotted curves from top to bottom.

The phase of the total amplitude in the asymptotic limit is

$$\arg [M_{\epsilon_k, \epsilon_i}^{(2)}] = \pi + \arg [Y_{l,m}(\hat{k})] + \phi_\Omega + \phi_\omega - \frac{\pi}{2}(l' - |l_2|) + \eta_{l'(\kappa)} + \phi_{cc}(k, \kappa), \quad (10)$$

where, ϕ_Ω and ϕ_ω are the phases of the pump and probe pulses; respectively. The quantum phase associated with the CC transition is

$$\phi_{cc}(k, \kappa) = \arg \left[\frac{(2\kappa)^{\frac{iZ}{\kappa}}}{(2k)^{\frac{iZ}{k}}} \times \frac{\Gamma [2 + |l_2| + iZ(\frac{1}{\kappa} - \frac{1}{k})]}{(\kappa - k)^{iZ(\frac{1}{\kappa} - \frac{1}{k})}} \right]. \quad (11)$$

Note that, ϕ_{cc} originates from the absorption of the vortex IR pulse in the presence of the Coulomb potential Z . It is important to notice that the vortex nature of the IR pulse ($|l_2|$) appears in the argument of the Gamma function, independently of the initial atomic state. If one substitutes $l_2 = 0$, the expression of ϕ_{cc} reduces to the known expression as reported in Eq. (22) in Ref. [33].

The calculation of the two-photon transition matrix element corresponding to the emission of the IR photon is similar, only the phase of the CC transition is opposite to the case

of the IR absorption.

The CC-phases for the different values of the OAM of the IR pulse are presented in Fig. 2. The solid and dotted lines correspond to the absorption and emission of an IR photon, for the same final kinetic energy, respectively. The phases are positive for absorption and negative for emission; whereas the magnitudes of the CC-phases are not exactly equal as evident from the figure. For low kinetic energies of the photoelectron, the phases increase with increasing the OAM. For high energies, the phases become insensitive to the OAM and approach those for regular light with zero OAM, as reflected in the figure.

The insensitivity of ϕ_{cc} to OAM for high kinetic energies follows from the fact that the dominant complex-valued and energy-dependent part of the two-photon transition amplitude comes from the phase of the Gamma-function. Since $(\frac{1}{\kappa} - \frac{1}{k}) \rightarrow 0$ as $k \rightarrow \infty$, $iZ(\frac{1}{\kappa} - \frac{1}{k}) \rightarrow 0$ in the argument of the Gamma function, which becomes real-valued.

RESULTS AND DISCUSSION

An experimental way to probe the quantum phase associated with CC-transition is offered by the RABBITT method. In this method, an XUV or x-ray attosecond pulse train is used as a pump pulse, with the photoelectron probed by the IR pulse. The pump-probe delay-dependent changes in the photoelectron spectrum give access to the sub-IR-cycle temporal resolution. In RABBITT, the same final state can be reached by two paths: either an absorption of pump photon [(2q-1)-th harmonic] followed by an absorption of an IR photon ($\omega\tau = \phi_\omega$) or an absorption of pump photon [(2q+1)-th harmonic] followed by an emission of an IR photon with phase ($-\omega\tau = -\phi_\omega$). Both quantum paths lead to the same final ‘sideband’ state at the energy of the 2q-th harmonics. The phase-dependent interferences of the two paths yield the oscillations in the intensity of the sideband, which is written in terms of the interference of the two-photon transition amplitudes corresponding to absorption $M^{(a)}$ and emission of an IR photon $M^{(e)}$ as $\mathcal{I}_{2q} = |M^{(a)} + M^{(e)}|^2$. The interference-term of \mathcal{I}_{2q} encodes the phase as

$$\arg(M^{(a)}M^{(e)}) \approx -2\omega\tau + \phi_{2q+1} - \phi_{2q-1} + \eta_{l'}(\kappa_{<}) - \eta_{l'}(\kappa_{>}) + \phi_{cc}(k, \kappa_{>}) - \phi_{cc}(k, \kappa_{<}). \quad (12)$$

Here $(-2\omega\tau + \phi_{2q+1} - \phi_{2q-1})$ -term contains the phase of the field. The finite-difference version of the Wigner-Smith time-delay is expressed in terms of the scattering phase: $\tau_{l'}^{\text{WS}}(k) =$

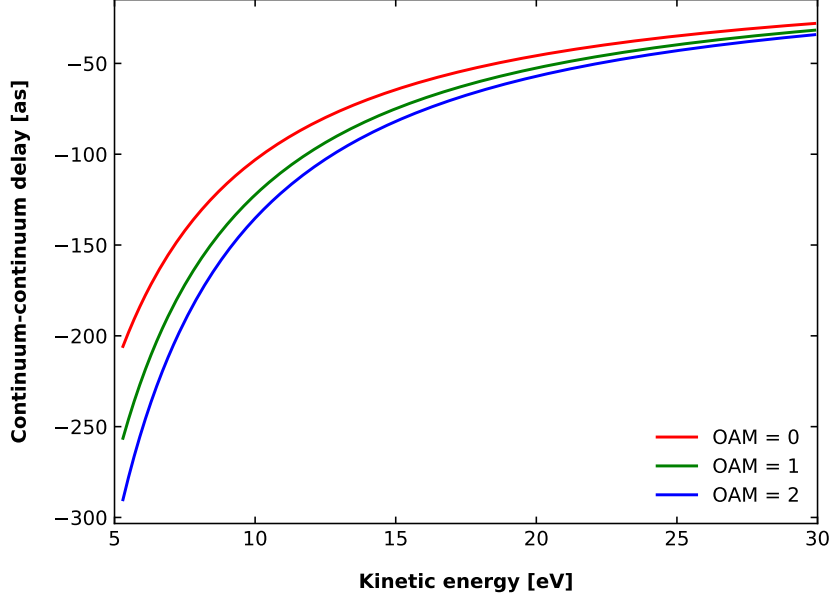


FIG. 3: The time-delays corresponding to continuum-continuum transitions, τ_{cc} , for different OAM values of the vortex IR pulse with $\omega = 1.55$ eV and $Z = 1$. Here, OAM = 0 corresponds to regular IR pulse. The legend represents the solid curves from bottom to top and the dotted curves from top to bottom.

$[\eta'(\kappa_{<}) - \eta'(\kappa_{>})]/(2\omega)$ and the time-delay corresponding to the CC-phase is

$$\tau_{cc}(k) \approx \frac{\phi_{cc}(k, \kappa_{>}) - \phi_{cc}(k, \kappa_{<})}{2\omega}. \quad (13)$$

The CC time delay is the finite difference approximation for the derivative of ϕ_{cc} with respect to 2ω in RABBITT. It can be seen that τ_{cc} is universal and independent of the initial and final angular momenta states of the atom. Here, $\epsilon_{<} = \epsilon_i + (2q - 1)\omega = \kappa_{<}^2/2$ and $\epsilon_{>} = \epsilon_i + (2q + 1)\omega = \kappa_{>}^2/2$ are the energies of the two quantum paths.

Figure 3 presents τ_{cc} for different values of OAM of vortex IR pulse. In general, τ_{cc} increases monotonically as a function of kinetic energy but remains negative: the photoelectron appears to be ahead compared to the electron moving in the absence of the core potential. In the relatively low kinetic energy regime, τ_{cc} becomes more negative for a larger value of OAM. The delays merge to a constant value as the kinetic energy increases.

CONCLUSION

In conclusion, we have developed the theory of time-resolved photoionization induced by a vortex pulse carrying OAM. The main finding of this study is the impact of the OAM of the probe beam on photoionization delays. As in a standard RABBITT setup, the total phase associated with the ionization process is a sum of the two phases, the scattering phase associated with the bound-free transition induced by the pump pulse and the CC phase associated with the transition induced by the IR pulse. The CC phase depends parametrically on the OAM of the vortex pulse and the charge of the remaining ionic core. The CC phase does not depend on the angular momentum states of the system and the short-range behaviour of the atomic potential. Our theory can also be used for other interferometric photoionization measurement methods such as the attosecond streaking camera for relatively low IR intensity as discussed in Ref. [33]. The present work provides a step towards attosecond chronoscopy of photoionisation in twisted light beams. Other important effects such as spatial sampling for specific focusing conditions, better description of the continuum wavefunction to include electron-electron correlations (e.g., in the vicinity of autoionizing states) etc. need to be incorporated in specific experiments for simulations of RABBITT and streaking spectra.

ACKNOWLEDGEMENTS

G.D. acknowledges support from Science and Engineering Research Board (SERB) India (Project No. ECR/2017/001460) and Max-Planck India visiting fellowship. M.I. acknowledges DFG QUTIF program, Grant IV 152/6-2.

* gdixit@phy.iitb.ac.in

- [1] L. Allen, M. W. Beijersbergen, R. J. C. Spreeuw, and J. P. Woerdman, *Phys. Rev. A* **45**, 8185 (1992).
- [2] F. Cardano and L. Marrucci, *Nature Photonics* **9**, 776 (2015).
- [3] J. P. Torres and L. Torner, Twisted photons: applications of light with orbital angular momentum, John Wiley & Sons, 2011.

- [4] M. Babiker, D. L. Andrews, and V. E. Lembessis, *Journal of Optics* **21**, 013001 (2018).
- [5] J. Wang et al., *Nature Photonics* **6**, 488 (2012).
- [6] S. Fürhapter, A. Jesacher, S. Bernet, and M. Ritsch-Marte, *Optics Letters* **30**, 1953 (2005).
- [7] K. A. Forbes, *Phys. Rev. Letts.* **122**, 103201 (2019).
- [8] W. Brullot, M. K. Vanbel, T. Swusten, and T. Verbiest, *Science advances* **2**, e1501349 (2016).
- [9] K. A. Forbes and D. L. Andrews, *Optics Letters* **43**, 435 (2018).
- [10] A. M. Yao and M. J. Padgett, *Advances in Optics and Photonics* **3**, 161 (2011).
- [11] M. F. Andersen, C. Ryu, P. Cladé, V. Natarajan, A. Vaziri, K. Helmerson, and W. D. Phillips, *Phys. Rev. Letts.* **97**, 170406 (2006).
- [12] R. Inoue, N. Kanai, T. Yonehara, Y. Miyamoto, M. Koashi, and M. Kozuma, *Physical Review A* **74**, 053809 (2006).
- [13] M. Zürch, C. Kern, P. Hansinger, A. Dreischuh, and C. Spielmann, *Nature Physics* **8**, 743 (2012).
- [14] C. Hernández-García, A. Picón, J. San Román, and L. Plaja, *Phys. Rev. Letts.* **111**, 083602 (2013).
- [15] G. Gariepy, J. Leach, K. T. Kim, T. J. Hammond, E. Frumker, R. W. Boyd, and P. B. Corkum, *Phys. Rev. Lett.* **113**, 153901 (2014).
- [16] R. Généaux, A. Camper, T. Auguste, O. Gobert, J. Caillat, R. Taïeb, and T. Ruchon, *Nature Communications* **7**, 12583 (2016).
- [17] L. Rego, J. San Román, A. Picón, L. Plaja, and C. Hernández-García, *Phys. Rev. Letts.* **117**, 163202 (2016).
- [18] A. Turpin, L. Rego, A. Picón, J. San Román, and C. Hernández-García, *Scientific Reports* **7**, 43888 (2017).
- [19] C. Hernández-García, A. Turpin, J. San Román, A. Picón, R. Drevinskas, A. Cerkauskaitė, P. G. Kazansky, C. G. Durfee, and Í. J. Sola, *Optica* **4**, 520 (2017).
- [20] W. Paufler, B. Böning, and S. Fritzsche, *Physical Review A* **98**, 011401 (2018).
- [21] D. Gauthier et al., *Optics Letters* **44**, 546 (2019).
- [22] D. Gauthier, P. R. Ribič, G. Adhikary, A. Camper, C. Chappuis, R. Cucini, L. F. DiMauro, G. Dovillaire, F. Frassetto, R. Généaux, P. Miotti, L. Poletto, B. Ressel, C. Spezzani, M. Stuppar, T. Ruchon, and G. D. Ninno, *Nature Communications* **8**, 14971 (2017).
- [23] F. Kong, C. Zhang, F. Bouchard, Z. Li, G. G. Brown, D. H. Ko, T. J. Hammond, L. Arissian,

- R. W. Boyd, E. Karimi, and P. B. Corkum, *Nature Communications* **8**, 14970 (2017).
- [24] K. M. Dorney et al., *Nature Photonics* **13**, 123 (2019).
- [25] C. T. Schmiegelow, J. Schulz, H. Kaufmann, T. Ruster, U. G. Poschinger, and F. Schmidt-Kaler, *Nature Communications* **7**, 12998 (2016).
- [26] R. Pazourek, S. Nagele, and J. Burgdörfer, *Rev. Mod. Phys.* **87**, 765 (2015).
- [27] A. Picón, A. Benseny, J. Mompart, J. R. V. de Aldana, L. Plaja, G. F. Calvo, and L. Roso, *New Journal of Physics* **12**, 083053 (2010).
- [28] A. Picón, J. Mompart, J. R. V. de Aldana, L. Plaja, G. F. Calvo, and L. Roso, *Optics Express* **18**, 3660 (2010).
- [29] M. Babiker, C. R. Bennett, D. L. Andrews, and L. C. D. Romero, *Physical Review Letters* **89**, 143601 (2002).
- [30] A. A. Peshkov, D. Seipt, A. Surzhykov, and S. Fritzsche, *Physical Review A* **96**, 023407 (2017).
- [31] F. Giammanco, A. Perona, P. Marsili, F. Conti, F. Fidecaro, S. Gozzini, and A. Lucchesini, *Optics Letters* **42**, 219 (2017).
- [32] J. Wätzel and J. Berakdar, *Phys. Rev. A* **94**, 033414 (2016).
- [33] J. M. Dahlström, D. Guénot, K. Klünder, M. Gisselbrecht, J. Mauritsson, A. L'Huillier, A. Maquet, and R. Taïeb, *Chemical Physics* **414**, 53 (2013).